

Universidade Federal de Viçosa - UFV

Centro de Ciências Exatas e Tecnológicas - CCE

Departamento de Engenharia Elétrica - DEL

SOLAR ARRAY EMULATORS: AN OVERVIEW

Wesley Venancio Ribeiro

Orientador : Prof. Dr. Heverton Augusto Pereira

Co-orientadora : Eng. Shirleny Pedrosa Silveira

Viçosa, May 3rd, 2018.

Universidade Federal de Viçosa - UFV

Centro de Ciências Exatas e Tecnológicas - CCE

Departamento de Engenharia Elétrica - DEL

SOLAR ARRAY EMULATORS: AN OVERVIEW

Wesley Venancio Ribeiro

Trabalho de Conclusão de Curso submetido ao Departamento de Engenharia Elétrica da Universidade Federal de Viçosa para a obtenção dos créditos referentes à disciplina Monografia e Seminário do curso de Engenharia Elétrica.

Orientador : Prof. Dr. Heverton Augusto Pereira

Co-orientadora : Eng. Shirleny Pedrosa Silveira

Viçosa, May 3rd, 2018.


WESLEY VENÂNCIO RIBEIRO

SOLAR ARRAY EMULATORS: AN OVERVIEW

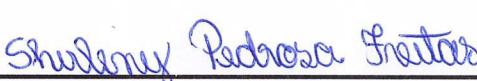
Monografia apresentada ao Departamento de Engenharia Elétrica do Centro de Ciências Exatas e Tecnológicas da Universidade Federal de Viçosa, para a obtenção dos créditos da disciplina ELT 490 – Monografia e Seminário e cumprimento do requisito parcial para obtenção do grau de Bacharel em Engenharia Elétrica.

Aprovada em 03 de Maio de 2018.

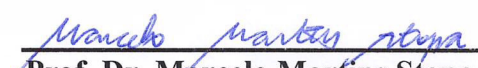
COMISSÃO EXAMINADORA



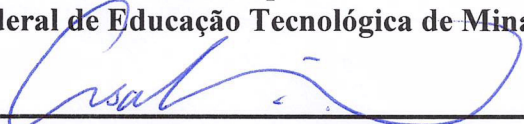
Prof. Dr. Heverton Augusto Pereira - Orientador
Universidade Federal de Viçosa - UFV



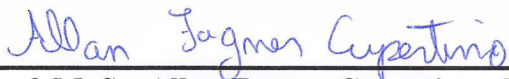
Eng^a. Shirleny Pedrosa Freitas - Coorientadora
Mestranda no Centro Federal de Educação Tecnológica de Minas Gerais - CEFET-MG



Prof. Dr. Marcelo Martins Stopa - Membro
Centro Federal de Educação Tecnológica de Minas Gerais - CEFET-MG



Prof. Dr. Alex Sander Amável Luiz - Membro
Centro Federal de Educação Tecnológica de Minas Gerais - CEFET-MG



Prof. M. Sc. Allan Fagner Cupertino - Membro
Centro Federal de Educação Tecnológica de Minas Gerais - CEFET-MG

*À minha família e
aos meus amigos.*

“Experience is what you get when you didn’t get what you wanted. And experience is often the most valuable thing you have to offer”

Randy Pausch

Agradecimentos

Primeiramente, quero agradecer a Deus e aos meus pais, Geraldo e Sueli, pelo suporte incondicional. Obrigado pela confiança em mim e por acreditarem sempre nos meus sonhos. Aos meus irmãos Larissa e Leonardo e ao meu sobrinho Gabriel por sempre minha base. Ao meu melhor amigo, Guilherme, por estar comigo durante os momentos mais difíceis da graduação. Aos meus amigos da Física por apoiarem minha mudança de curso. A minha parceira de pesquisa, Shirleny, pela experiência que me passou e pela confiança no meu trabalho. A todos os amigos de engenharia, república, intercâmbio e aos demais que contribuíram para essa conquista. Ao professor Heverton, por incentivar a pesquisa e o desenvolvimento dos alunos. Obrigado ao GESEP, pelo amadurecimento e experiência.

Summary

Resumo	xi
Abstract	xiii
Figures List	xvi
Tables List	xvii
1 Introduction	1
1.1 Context and Relevance	1
1.2 Certification	2
1.3 Literature	3
1.4 Objectives	4
1.5 Text Organization	5
2 Real Photovoltaic Array behaviorand Mathematical Model	7
2.1 The Photovoltaic Module	7
2.1.1 The Photovoltaic Cell	7
2.1.2 Choice of the Photovoltaic Cell Model	8
2.1.3 Mathematical Model Equations	11
3 SAS Models	15

3.1	SAS Topologies	16
3.1.1	SAS based on Thevenin's Circuit	16
3.1.2	SAS Based on buck converter	17
3.1.3	SAS Based on PWM Rectifier and Buck Converter	21
4	Adjustment of the Parameters Used in the Tests	27
4.1	PV Inverter Model	28
4.2	Studies Applied to Test the SAS	32
5	Results	33
5.1	Simulation Results	33
5.1.1	Irradiance Variation	33
5.2	Discussion	35
5.3	General Analysis	38
6	Conclusion	39
6.1	Published Works	40
	Referências Bibliográficas	43

Resumo

Nos últimos anos, o esgotamento contínuo dos recursos energéticos convencionais e o custo instável dos combustíveis têm motivado pesquisas sobre fontes alternativas de geração de energia. A energia solar sendo o principal entre todos os outros recursos de energia renovável evoluiu como um substituto confiável para a geração de energia convencional. Um elemento fundamental no controle de sistemas fotovoltaicos conectados à rede é o conversor eletrônico conhecido popularmente como inversor. Este componente tem como principal função injetar toda a potência gerada pelos painéis fotovoltaicos (PV) na rede elétrica. No entanto, para que possam ser comercializados, os conversores eletrônicos devem ser testados, certificados de acordo com as normas vigentes e receber o selo de conformidade do INMETRO. No processo de certificação, é utilizado um equipamento conhecido como emulador de módulos fotovoltaicos (Solar Array Simulator - SAS). Ao contrário de outras fontes, a pesquisa em tempo real em sistemas PV é uma tarefa específica uma vez que requer o uso desse painel solar artificial (emulador) que tem a função de replicar com precisão as características não-lineares de uma célula fotovoltaica. Pesquisadores desenvolveram emuladores de diferentes tipos utilizando diversas configurações. Neste contexto, este trabalho tem como objetivo principal apresentar diferentes topologias de painel solar artificial. Um modelo matemático é apresentado e utilizado como parâmetro para a validação dos outros modelos. Os emuladores de painel fotovoltaico foram analisados durante a variação de irradiância e também de temperatura dos painéis. Os três modelos apresentados seguiram a referência e apresentaram a capacidade de seguir o ponto de máxima potência da curva $I \times V$.

Abstract

In recent years, the continued depletion of conventional energy resources and the unstable cost of fuel has motivated research on alternative sources of energy generation. Solar energy is currently one of the most popular and renewable energy resource on the earth. Thus, photovoltaics (PV) in particular are receiving significant research attention in terms of developing the PV system to improve efficiency and to meet grid codes, as well as developing intelligent methods of control. Once PV inverters are a fundamental device in PV applications, it must be tested according to standards in order to be certified and commercialized. A common practice to test PV inverters is the utilization of solar array simulators (SAS). Nevertheless, the research on SAS is a difficult assignment as it has nonlinear characteristics. In literature, many works have developed emulators of different type utilizing various configurations. This work attempts to present some SAS topologies, responsible to emulate the photovoltaic array behavior. A mathematical model is presented and used as a parameter for the validation of the other models. The photovoltaic panel emulators were analyzed during the irradiance variation and also the temperature of the panels. The three models of SAS followed the reference, and presented the ability to follow the maximum power point of the $I \times V$ curve.

Lista de Figuras

1.1	Electricity capacity additions	2
2.1	Equivalent electric circuit of a photovoltaic cell model	8
2.2	Electrical behavior of the photovoltaic module equivalent circuit	9
2.3	Characteristic curves of the panel modeled for different levels of irradiance and temperature: (a) I x V curve for T = 25°C and various irradiance values; (b) P x V curve for T = 25°C and various irradiance values; (c) I x V curve for G = 1000 W/m ² and various temperature values of the module; (d) P x V curve for G = 1000 W/m ² and various temperature values of the module.	10
3.1	General diagram of a grid-tie photovoltaic system	15
3.2	Topologies of Solar Panel (a) PV Panel Model (b) SAS based on Thevenin's Circuit (c) SAS based on buck converter (d) SAS Based on PWM Rectifier and Buck Converter	16
3.3	Structure solar array simulator with resistive loads (Temperature = 25°C).	17
3.5	Panel emulator stage d.c./d.c. model.	18
3.4	Estrutura de emulador de gerador fotovoltaico com cargas resistivas.	18

3.6	Complete control structure of d.c./d.c. converter.	19
3.7	Structure of solar array simulator.	21
3.8	Complete Control structure of PWM rectifier.	23
4.1	Grid-connected photovoltaic system based on three-phase multifunctional inverter	29
4.2	Complete inverter control strategy	30
5.1	Electrical Variables of the Artificial Panel during a variation of irradiance and constant temperature (25°C). (a) SAS output current. (b) SAS output voltage. (c) SAS output power.	34
5.2	Electrical variables of the artificial panels during a temperature variation (20°C to 30°C to 40°C) and constant irradiance (1000 W/m ²). (a) SAS Output current. (b) SAS Output voltage. (c) SAS Output power.	36
5.3	(a) SAS track during the test of a photovoltaic converter in the P x V plane. (b) maximum power point zoom.	37

Lista de Tabelas

2.1	Solar panel parameters supplied by the manufacturer	9
4.1	Parameters of the solar panel	28
4.2	D.c./d.c. Stage Parameters	29
4.3	A.c./a.c. Stage Parameters	30

Introduction

Exhaustion of conventional energy reserve and alarming environmental concerns has instigated the necessity to find a substitute for traditional power generation (Solanki, 2015). With low environmental threat, solar energy has gained universal attention for its huge potential (Babu et al., 2016). Moreover, eco-friendly renewable power generation is considered to be an important asset for the mankind.

1.1 Context and Relevance

The installation of solar photovoltaic (PV) power plants have increased considerably around the world in the last decades. The installed and commissioned power in PV systems reach 76.6 GW in 2016, showing a growth of 51.4% over the 50.6 GW commissioned in 2015 (EPIA et al., 2017). For the first time, solar PV additions rose faster than any other fuel, surpassing the net growth in coal as can be seen in Figure 1.1.

The cumulative installed solar PV power capacity increases year-on-year, at the same time that the PV system prices declines of around 75% in less than 10 years (EPIA et al., 2017). However, with the progress of the renewable energy, including the photovoltaic sources, the concern about the grid power quality grows too, mainly due to the use of power electronic based-converters.

A grid-connected PV system consists of several components, including solar panels to absorb and convert sunlight into electricity, a solar inverter to

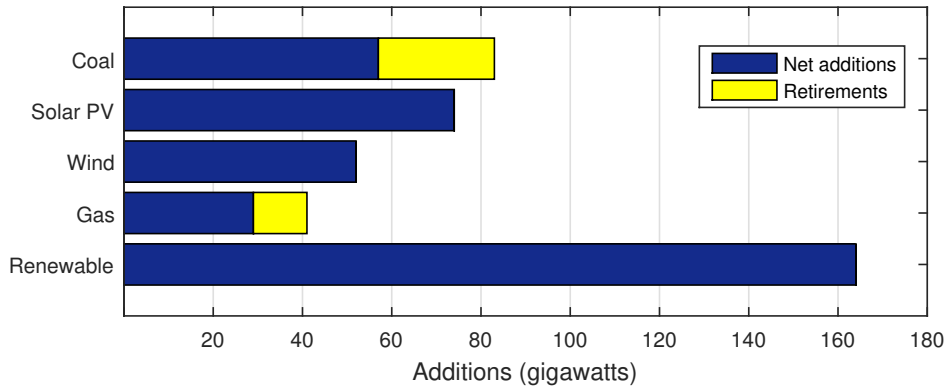


Figura 1.1: Electricity capacity additions

Fonte: (EPIA et al., 2017)

change the electric current from direct current (d.c.) to alternating current (a.c.), as well as mounting, cabling, and other electrical accessories to set up a working system. The fundamental element of these systems is the inverter, which injects the generated power into the power system. This device is able to improve the quality of the power delivered to the grid.

Due to its importance in PV system, power inverters for PV applications must be tested and certified according to standards before being commercialized (Camino-Villacorta et al., 2012). The test procedure standards for inverters connected to the grid were defined based on the minimum requirements to be demanded of these equipments. Each country has specific requirements and regulations to certify PV inverters.

1.2 Certification

Two documents stand out internationally as references for certification of photovoltaic inverters. The first is the IEC 61683 standard, which already introduces the concept of Solar Array Simulator (SAS). SAS is a simulator able to reproduce an $I \times V$ characteristic equivalent to a real PV array (IEC, 1999). The second document was prepared by the Sandia laboratories in the

United States and attempts to establish a test procedure for performance of photovoltaic inverters evaluation (Bower et al., 2004). The Sandia Laboratories are notable for the great scientific production and bibliography on the photovoltaic field (Boyson et al., 2007).

In Brazil, these requirements and procedures are indicated in the standards ABNT NBR 16149: 2013, ABNT NBR 16150: 2013, and ABNT NBR IEC 62116: 2012. They are based on International Electrotechnical Commission (IEC) standards, and contain guidelines for performing inverter efficiency tests. In these documents, it is possible to find guidelines for the performance of inverter efficiency tests, as well as the defined instruments of measurement, their ranges of uncertainty and necessary precision.

The use of photovoltaic arrays in the test is a methodology few flexible since the weather conditions are not controlled. Moreover, the array needs to be reconfigured in order to test inverters with different rated power. For this reason, IEC 61683 suggests the use of a SAS in the certification tests. As mentioned, this device is a power source which reproduces I-V (Current-Voltage) characteristics similar to a real PV array (IEC, 1999). SAS can emulate the solar array behavior for a set of weather conditions (e.g. irradiance and temperature) and partial shadowing. Furthermore, this device can operate with different power levels and can be used to test inverters with different rated power.

Most commercial inverters control the solar array output voltage in order to track the maximum power point (Di Piazza et al., 2010). Therefore, the SAS output voltage is controlled by the inverter under test. Since the purpose of the SAS is to reproduce the I-V characteristic of a solar array, its output current must be controlled by this simulator.

1.3 Literature

Several SAS topologies for low-power applications are presented in literature. Starting with the simplest, in (Pandey et al., 2007) is proposed a low cost option to a SAS based on a variable dc power supply. Although this topology is simple, it uses a series resistor that increases the system losses. In (Nagayoshi, 2004), it is proposed a magnifier circuit applied to a photo

sensor that obtains characteristics of a solar array. At last, in (Gadelovits et al., 2014), it is proposed an adaptation in a commercial dc power supply in order to build a SAS. Basically, the output current is sensed, processed by a microcontroller which defines the dc power supply voltage reference.

Generally, the SAS topologies present two stages: a rectifier stage based on diodes and a dc/dc converter. The dc/dc buck converter is the most employed in the literature (Ollila, 1995); (Matsukawa et al., 2003); (Gonzalez et al., 2010); (Bun et al., 2011); (Piao et al., 2013); (Di Piazza et al., 2010). A low cost SAS based on buck converter is proposed in (Vijayakumari et al., 2012). However, the converter design considers only the nominal operation point of the converter and the experimental results considered only resistive loads connected to the SAS output.

Many works in literature design the d.c./d.c. power stage considering only the nominal operation point (Cupertino et al., 2012). This approach is widely used for applications in which the converter works with a constant output voltage ((Erickson and Maksimovic, 2007), (Soltau et al., 2015)). However, due to variations in the operation point on the solar array curve, the converter design needs to include an analysis in other operation points. Based on the mentioned limitations, an improved SAS structure is presented in (Cupertino et al., 2015), (Cupertino et al., 2015), which is used in this work.

1.4 Objectives

As seen, various scholarly research employing assorted methodologies are available for design of PV emulator. However, there is no published work up to date in consolidating the efforts. Moreover, no attempts were made to even list the works and summarize the contributions. Hence in this work, the author presents some models and shows their performance in simulations with different weather conditions. The contributions of this work are:

- Presentation of three different SAS topologies;
- Simulation of those SAS connected to PV array;

- Analysis of three SAS operation dynamics when connected in a grid-tie PV inverter.

1.5 Text Organization

This work is divided into six chapters. In chapter 2, it is chosen the photovoltaic cell model to be studied and mathematical models associated with it.

Chapter 3 introduces the SAS models. It intends to show the topologies of the emulators. Initially, a review is presented on the modeling of photovoltaic modules. Then, the topologies of emulators of photovoltaic generator that are addressed throughout this work are shown as well the modeling and control structures.

The fourth chapter presents a case study to analyze the dynamical behavior of the models, both in conditions of irradiance and temperature variations. In addition, it presents the modeling and control structures of a 10 kW photovoltaic inverter, which was used as a test in the computational simulations.

Chapter 5 presents the computational simulation results obtained with the use of the models developed in the previous chapters. Finally, in Chapter 6, the conclusions and proposals for the continuity of this work are stated.

Real Photovoltaic Array behavior and Mathematical Model

Over the decades, the introduction of emulators has remarkably contributed to increased utilization of solar energy. In addition, the emulator design arena has witnessed a phenomenal uplift starting from basic mathematical model approximation to real time controller implementations in recent times.

This chapter intends to present a mathematical model of a solar array. It is shown an equivalent electric circuit of a photovoltaic module as well its electrical behavior. First, it is chosen a photovoltaic cell model to be studied and knowing the phenomena and, then, the mathematical model associated with it.

2.1 The Photovoltaic Module

2.1.1 The Photovoltaic Cell

A solar cell, or photovoltaic cell, is an electrical device that converts the energy of light directly into electricity by the photovoltaic effect, which is a physical and chemical phenomenon. Commonly, these cells generate powers in the range of 1 to 2 W, such that it is possible to obtain higher voltage and current values from the union of several cells connected in series or parallel

in photovoltaic modules (CRESESB, 2014).

The first step in the development of this work is the choice of the photovoltaic cell model to be studied. It is very important knowing the phenomena and mathematical models associated with it. In the literature various works are found with different modeling and different degrees of complexity for the description of the I-V characteristic of photovoltaic cells.

2.1.2 Choice of the Photovoltaic Cell Model

In (Souza et al., 2013) a model considering the parallel resistance, R_P , is used as shown in Figure 2.1. R_S represents the series resistance corresponding to resistive losses in the semiconducting material. R_P represents the parallel resistance, corresponding to the losses that occur between the layers of junction p-n of the semiconducting material (Souza et al., 2013).

The photovoltaic conversion efficiency is sensitive to changes in R_S ; however, it also has little sensitivity to variations in R_P . A small increase in R_S can reduce the panel output significantly.

The electrical behavior of a real photovoltaic panel can be represented by the circuit of Figure 2.1. This circuit results in the electrical behavior shown in Figure 2.2. The following notable points can be observed:

- The open-circuit point of the module ($V_{oc}, 0$);
- The short-circuit point of the module ($0, I_{sc}$);

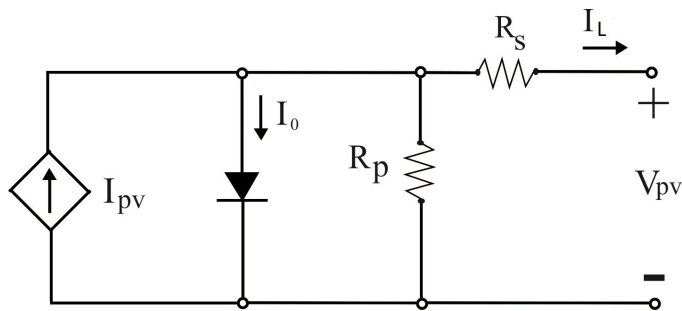


Figura 2.1: Equivalent electric circuit of a photovoltaic cell model

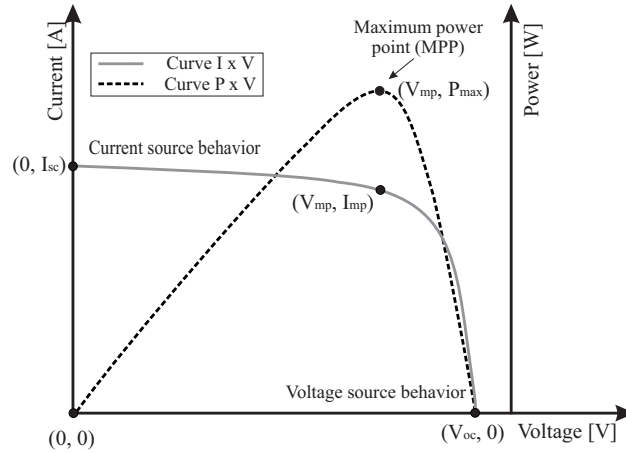


Figura 2.2: Electrical behavior of the photovoltaic module equivalent circuit

- The point of maximum power of the module (V_{mp} , I_{mp}).

Table 1 shows the main PV panel parameters provided by the manufacturers in commercial datasheets. Furthermore, other information that are not reported such as series and parallel resistors, as well as the ideality constant of diodes, can be necessary during simulations. These information are calculated based on algorithms proposed in literature (Villalva et al., 2009).

Tabela 2.1: Solar panel parameters supplied by the manufacturer

<i>Parameters</i>	Symbol
Open Circuit Voltage	Vocn
Short Circuit Current	Iscn
Maximum Power Voltage	Vmp
Maximum Power Current	Imp
Maximum Power	Pmax
Coefficient of short-circuit current	ki
Coefficient of open-circuit voltage	kv
Resistance in series	Rs
Parallel Resistance	Rp
Constant diode ideality	m

Photovoltaic systems can contain several photovoltaic panels in series or parallel connections. The series connection of panels results in a larger

dc output voltage, and the parallel connection results in a larger dc output current.

The Figures 2.3 (a) and (b) show the characteristic I x V and P x V curves, respectively, for different irradiance values and at constant temperature of 25°C. Figures 2.3 (c) and (d) show the curves obtained for different temperature values and a constant irradiance of 1000 W/m². It is observed that the voltage value at the point of maximum power varies as a function of the levels of irradiance and, significantly, with the temperature of the module.

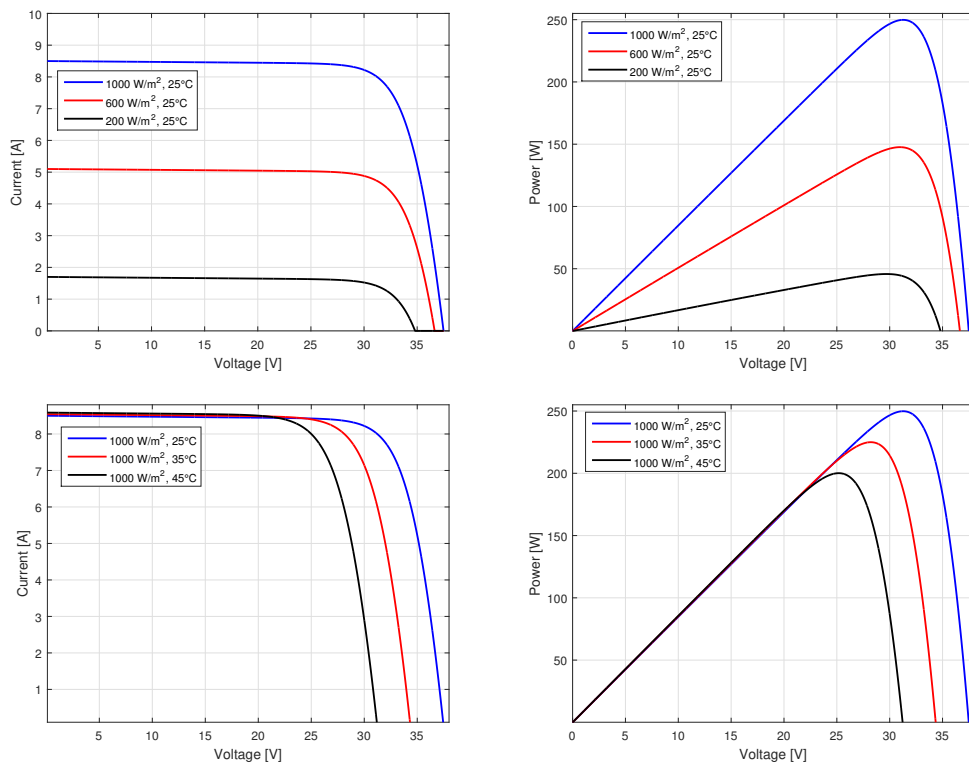


Figure 2.3: Characteristic curves of the panel modeled for different levels of irradiance and temperature: (a) I x V curve for $T = 25^{\circ}\text{C}$ and various irradiance values; (b) P x V curve for $T = 25^{\circ}\text{C}$ and various irradiance values; (c) I x V curve for $G = 1000 \text{ W/m}^2$ and various temperature values of the module; (d) P x V curve for $G = 1000 \text{ W/m}^2$ and various temperature values of the module.

2.1.3 Mathematical Model Equations

The mathematical model is taken from the electrical circuit of Figure 2.1, which will be used as reference for all presented topologies. As seen, the photovoltaic module can be modeled by a current source in parallel with a diode (Rauschenbach, 2012). The model of a diode with constant resistances presents a good relation of simplicity and precision (Villalva et al., 2009), and this will be used in this work.

The relation between the voltage and the output current of the photovoltaic module can be expressed by:

$$I = I_{pv} - I_0 \left[\exp \left(\frac{V + R_s I_L}{m V_t} \right) - 1 \right] - \frac{V + R_s I_L}{R_p} \quad (2.1)$$

where I_{pv} and I_0 are the photoelectric and reverse saturation currents of the diode, and I_L is the output current. R_s and R_p are respectively the equivalent series and parallel resistances of the modules and m is the diode ideality constant ($1 \leq m \leq 1.5$). For an ideal diode, $m = 1$ (De Soto et al., 2006).

The thermal voltage of the photovoltaic array with N_s cells connected in series is given by:

$$V_t = \frac{N_s k T}{q} \quad (2.2)$$

where k is the Boltzmann constant [$1.3806503 \times 10^{-23}$ J/K], T [K] is the p-n junction temperature and q is the electron charge [$1.60217646 \times 10^{-19}$ C]. When cells are connected in parallel, the current is increased. When cells are connected in series, they provide higher output voltages.

The I-V characteristic of the photovoltaic device shown in Figure 2.2 depends on the internal characteristics of the device (R_s , R_p) and external influences, such as irradiance level and temperature. The amount of incident light directly affects the generation of chargers and, consequently, the current generated by the device.

The light generated current (I_{pv}) of the cells is given by:

$$I_{pv} = (I_{pv_n} + K_i \Delta T) \frac{G}{G_n} \quad (2.3)$$

where ΔT is the operating temperature variation of the photovoltaic module and T_n is the nominal temperature. K_i [A/K] is the coefficient of photoelectric current variation caused by temperature. G is the irradiance and G_n is the nominal irradiance.

The diode reverse leakage current I_0 is:

$$I_0 = \frac{I_{sc_n} + K_i \Delta T}{\exp\left(\frac{V_{oc_n} + K_v \Delta T}{mV_t}\right) - 1} \quad (2.4)$$

where I_{sc_n} and V_{oc_n} are the short-circuit current and the open-circuit voltage at the standard conditions. K_v [V/K] is the coefficient of variation of open circuit voltage with temperature.

Two parameters remain unknown in equation (2.1), which are R_s and R_p . In this way Villalva et al. (2009) proposes a method for setting R_s and R_p based on the fact that there exists a unique pair R_s , R_p which guarantees that $P_{max,m} = P_{max,e} = V_{mp}I_{mp}$ at the point (V_{mp}, I_{mp}) of the IxV curve, that is, the maximum power calculated by the IxV model of equation (2.1), $P_{max,m}$, is equal to the maximum experimental power of *datasheet*, $P_{max,e}$. The relationship between R_s and R_p , can be found by making $P_{max,m} = P_{max,e}$, and solving the resulting equation to R_s and R_p , as shown by the equations (2.5) and (2.6).

$$P_{max,m} = V_{mp} \left\{ I_{pv} - I_0 \left[\exp\left(\frac{V_{mp} + R_s I_{mp}}{mV_t}\right) - 1 \right] - \frac{V_{mp} + R_s I_{mp}}{R_p} \right\} = P_{max,e} \quad (2.5)$$

$$R_p = \frac{V_{mp} (V_{mp} + R_s I_{mp})}{V_{mp} I_{pv} - V_{mp} I_0 \left[\exp\left(\frac{V_{mp} + R_s I_{mp}}{mV_t}\right) - 1 \right] + V_{mp} I_0 - P_{max,e}} \quad (2.6)$$

The objective is to find the value of R_s (and hence R_p) to get the maximum point of the mathematical curve PV, and it has to coincide with the

maximum point of the experimental curve (V_{mp}, I_{mp}) . It requires several iterations until $P_{max,m} = P_{max,e}$. In the iterative process, the values of R_s must be increased slowly starting from $R_s = 0$ (Villalva et al., 2009).

SAS Models

A PV inverter can be connected to photovoltaic panels under various operating conditions, depending of environmental behavior. However, this strategy is totally unacceptable under the validation and certification stages. Therefore, the use of a SAS is extremely important in carrying out inverter tests once irradiance and temperature profiles can be emulated.

Thus, a PV inverter can be tested operating in several conditions, with commands imposed by the operator. This procedure is much cheaper and more flexible than use PV panels submitted to environmental conditions.

This Chapter describes three PV emulators available in literature. Considering the great importance of a SAS, several authors have proposed different topologies of emulators to follow as best as possible the behavior of a real PV array. Figure 3.1 shows a photovoltaic system connected to the grid. The quantities to be supplied by the panel are current (i_{pv}) and voltage (v_{pv}).

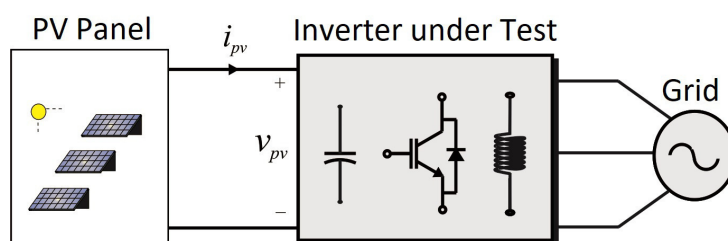


Figura 3.1: General diagram of a grid-tie photovoltaic system

3.1 SAS Topologies

In Figure 3.2, it can be seen the electrical circuit of some SAS topologies proposed in literature. In this work, these topologies are presented and simulated to analyze their capacity of emulate the $I \times V$ curves of solar arrays during irradiance variations. Fig. 3.2 (a) shows the mathematical model presented in the previous chapter. The other models are presented in this chapter.

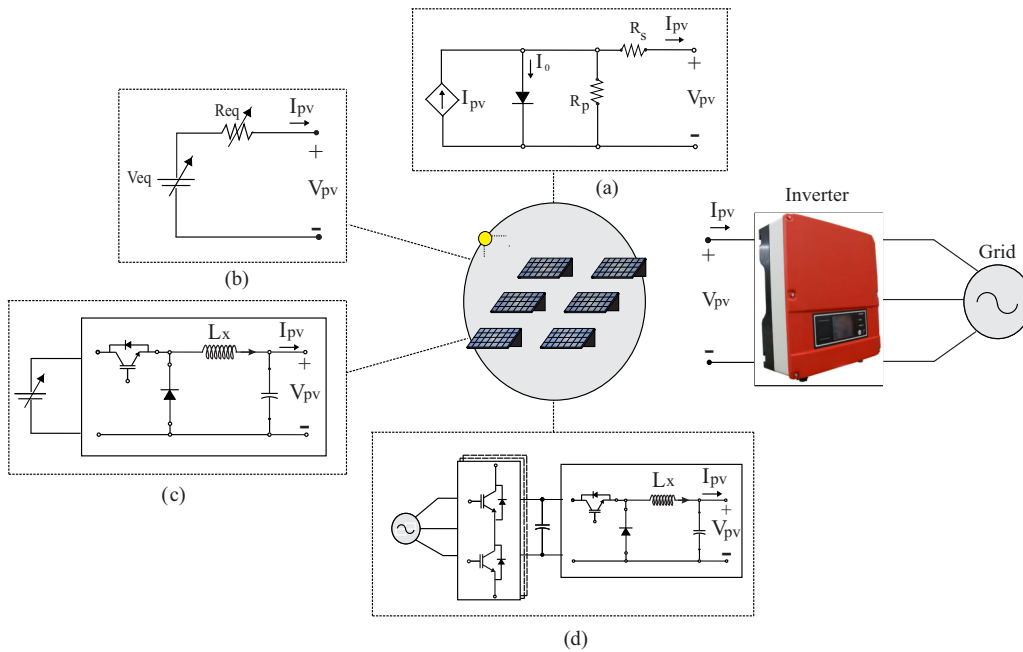


Figure 3.2: Topologies of Solar Panel (a) PV Panel Model (b) SAS based on Thevenin's Circuit (c) SAS based on buck converter (d) SAS Based on PWM Rectifier and Buck Converter

3.1.1 SAS based on Thevenin's Circuit

This is the simplest SAS topology based on the association of resistances in series with a dc adjustable voltage source. In Fig. 3.3, it is illustrated the non-linear $I \times V$ characteristic curve with the linear characteristic of the SAS based on Thevenin's circuit.

The circuit of Fig. 3.4 is valid at the linearization point (V, I) and is a good approximation of the PV array for small-signal analysis at the neighborhood of this point.

The values of voltage source and resistance for different values of temperature and irradiance can be calculated through equation (3.1) and (3.2).

$$V_{eq} = 2V_{MPPT} \quad (3.1)$$

$$R_{eq} = \frac{V_{MPPT}}{I_{MPPT}} \quad (3.2)$$

where V_{MPPT} e I_{MPPT} are the values of voltage and current in the maximum power point of the panel.

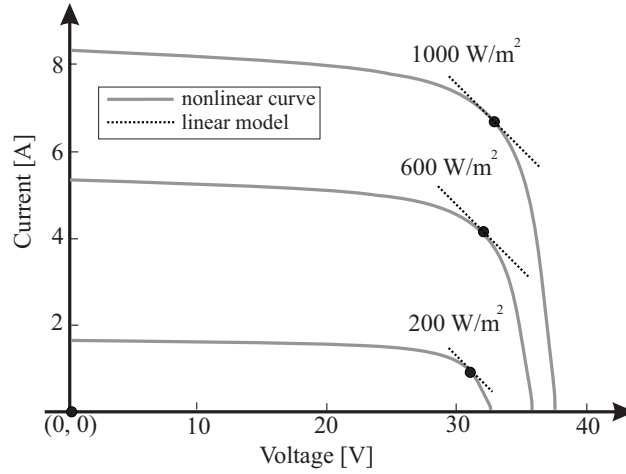


Figura 3.3: Structure solar array simulator with resistive loads (Temperature = 25°C).

3.1.2 SAS Based on buck converter

With the advancement of the studies, for a greater representation of a SAS, a photovoltaic arrangement simulator based on a buck converter is proposed, as shown in Fig. 3.5.

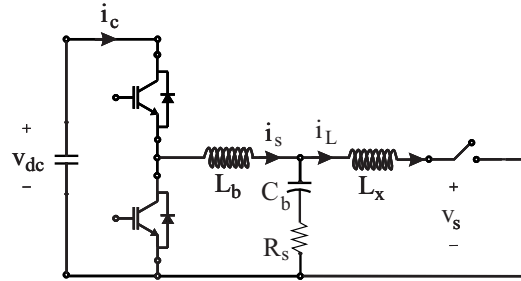


Figura 3.5: Panel emulator stage d.c./d.c. model.

The SAS proposed by (Cupertino, 2015) is shown in Figure 3.6. It is possible to see both operation modes: the open-circuit control mode is based on a proportional-integral (PI) compensator.

- Open-circuit control mode. It is responsible for controlling the output voltage of the SAS when it is unloaded. In this situation, a reference voltage is the open circuit voltage of the emulated solar array;
- Solar array simulator control mode. Based on the voltage imposed by the converter under the test, the current reference is obtained based on the look-up table from I-V curve.

In this work, it is used only the second operation mode once it does not have a practical part, just computer simulation.

The SAS control mode is based on a look-up table of $I \times V$ curves. This method consists in the following steps: for a given value of solar irradiance G and temperature T_c , a table with the values of an I-V curve is chosen.

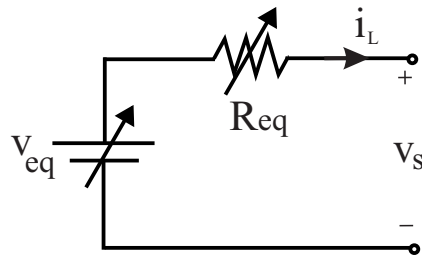


Figura 3.4: Estrutura de emulador de gerador fotovoltaico com cargas resistivas.

The value of the output voltage is interpolated in this table and the result is the reference value of the inductor current. This interpolation is performed dynamically (Matsukawa, 2003).

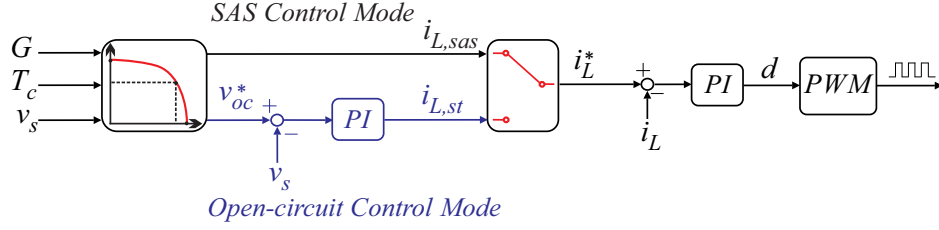


Figura 3.6: Complete control structure of d.c./d.c. converter.

Fonte: (Cupertino et al., 2015)

In the d.c./d.c. converter modeling, the following points are considered:

- The converter switches are driven in complementary;
- The dc bus voltage of the rectifier is constant;
- Only the ohmic losses in the inductor of the converter are considered.

The current controller is used in both control modes of the SAS using PI controller. The adjustment of the controllers is performed according to the methodology proposed by (Cupertino, 2015). A PI controller is also used in the voltage regulation circuit and adjusted by the pole allocation method. The proportional and integral gains of the current loop are given by:

$$k_{(p,iL)} = \frac{2\pi f_{c1}(L_b + L_x)}{V_{eb}}, \quad (3.3)$$

$$k_{(i,iL)} = \frac{2\pi f_{c1}(R_b + R_x)}{V_{eb}}, \quad (3.4)$$

where, f_{c1} is the cut-off frequency of the current loop. Its value is limited to two decades below the converter switching frequency. V_{dc} is voltage of cb.

Lb and Lx are the inductors of the buck converter, and Rb and Rx are the resistors of the inductor.

Similarly to the previous one, the proportional and integral gains of the voltage loop are given by:

$$k_{(p,v_s)} = 2\pi(f_{c2} + f_{c3})C_b, \quad (3.5)$$

$$k_{(i,v_s)} = 4\pi^2(f_{c2}f_{c3})C_b, \quad (3.6)$$

where, f_{c2} and f_{c3} are the frequencies of the closed loop equation. Typically these poles are separated from one another by a decade and the value of the largest of them must be allocated at least a decade below the cut-off frequency of the current loop. This is necessary to ensure proper operation of the cascade control. The digital implementation of the control uses a sampling time equal to the switching frequency (Erickson, 2004).

At the SAS output, a second inductor is inserted according to (Shirley, 2017). Therefore, the SAS LCL filter can be interpreted as two cascade LC filters. The resonance frequency of the LCL circuit associated with the inverter under test capacitance C_{min} (in radians per second), is given by:

$$\omega_{res1} = \sqrt{\frac{1}{L_X C_{min}}} \quad (3.7)$$

In order to avoid resonance problems, this resonance frequency is allocated between 10 times the fundamental frequency and 1/3 of the switching frequency. Therefore,

$$\omega_{res1} = \frac{2\pi f_{sb}}{3}. \quad (3.8)$$

Then, replacing (3.7) in (3.8) and isolating L_X , the value of this inductance can be found taking into account the resonance frequency and the minimum capacitor value of the inverter under test, thus:

$$L_X = \frac{1}{C_{min} \left(\frac{2\pi f_{sb}}{3} \right)^2}, \quad (3.9)$$

where f_{sb} is the switching frequency of the SAS. C_{min} is minimum value of the capacitance of the inverter under test. In this work this value was defined as 10 times smaller than the SAS output capacitor. L_b and C_b are calculated by (Cupertino et al., 2017).

3.1.3 SAS Based on PWM Rectifier and Buck Converter

In the previous simulator model, a dc source is used to represent the dc bus voltage, but the construction of a dc source is very expensive due to its high cost in the marketing. In view of this problem in this topology, the dc source is replaced by a three-phase PWM rectifier in cascade, as illustrated in Fig. 3.7

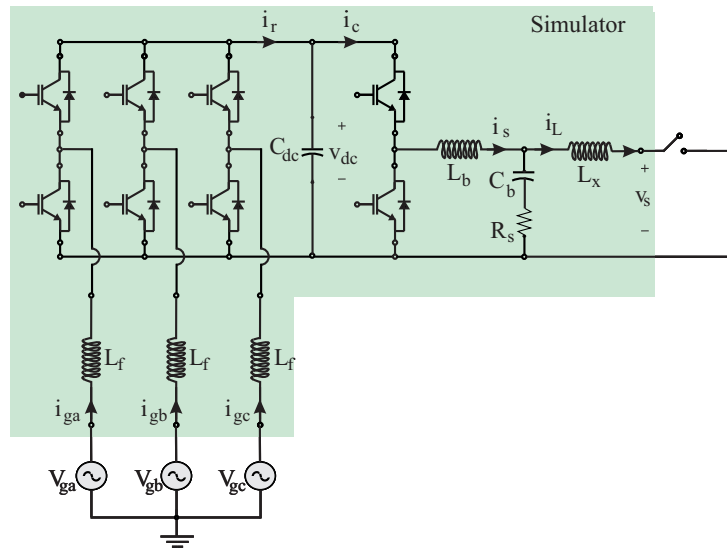


Figura 3.7: Structure of solar array simulator.

In this simulator structure of photovoltaic arrays, the modeling of the d.c./d.c. stage will be identical to that described in section 2.2. Beyond the

d.c./d.c. stage, the topology presents an a.c./d.c. stage, which is detailed below.

3.1.3.1 A.c/d.c. Stage

The SAS rectifier stage is based on a three-phase Pulse Width Modulation (PWM) converter. An inductive filter is used in order to reduce the harmonic content generated by the IGBTs switching. The design of this filter is presented in (Ponnaluri et al., 2000).

The classical control structure based on synchronous reference frame (dq) was employed to control the PWM rectifier. For the system modeling, grid voltages are considered balanced and without harmonic components. In this situation, the differential equations in the synchronous reference frame dq are written as:

$$v_d = -R_f i_d - L_f \frac{di_d}{dt} + \omega_n L_f i_q + v_{gd}, \quad (3.10)$$

$$v_q = -R_f i_q - L_f \frac{di_q}{dt} - \omega_n L_f i_d + v_{gq}, \quad (3.11)$$

where v_{gd} e v_{gq} are the direct and quadrature components of grid voltage, v_d and v_q are the components of the fundamental voltage generated by the rectifier, i_d and i_q are the components of the grid currents, L_f is the filter inductance and R_f is the filter resistance.

Synchronization of the converter with grid voltage is based on a Dual Second Order Generalized Integrator Phase-Locked Loop (DSOGI-PLL), proposed by (Rodriguez et al., 2006). This PLL has good responses for voltage unbalances and voltage harmonics. The modulation strategy implemented is the space vector PWM (SVPWM) technique.

The control structure consists in two cascade loops: internal loops controlling the direct and quadrature components of the grid currents and external loops regulate the dc bus voltage and the reactive power injected into the grid (Liserre et al., 2001). The control structure of PWM rectifier is presented in Fig. 3.8. The terms $\omega_{Ligd} + V_d$ and ω_{Ligq} are feedforward terms. The con-

trollers are adjusted according to the methodology presented in (Cupertino et al., 2015).

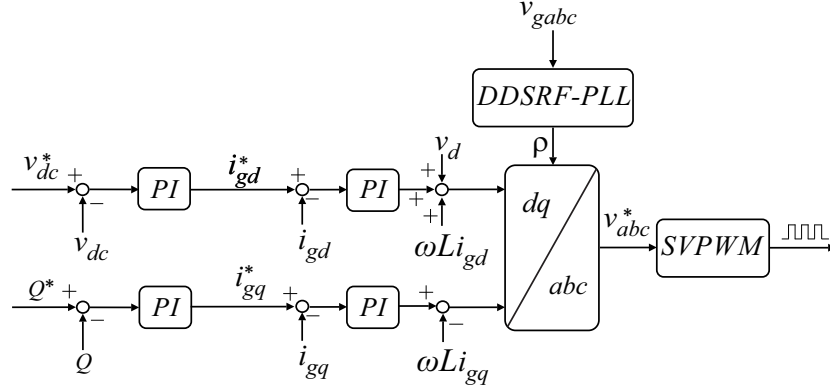


Figura 3.8: Complete Control structure of PWM rectifier.

Applying Laplace transform, it is obtained:

$$G_{id,q} = \frac{i_{d,q}(s)}{v_{rd,rq}(s)} = \frac{1}{L_f s + R_f} \quad (3.12)$$

Current loops use PI controllers adjusted by the pole allocation method. For the internal meshes, it results in the following gains:

$$k_{p,id,q} = 2\pi f_{dq} L_f \quad (3.13)$$

$$k_{i,id,q} = 2\pi f_{dq} R_f \quad (3.14)$$

where f_{dq} is the cutoff frequency of the current loops. Its value is usually limited to ten times the switching frequency.

The dynamic equation of the dc bus voltage is given by:

$$C_{dc} \frac{dv_{dc}}{dt} = i_r - i_c \quad (3.15)$$

where i_r is the rectified current and i_c is the current following to the d.c./d.c. stage.

The term i_c behaves like a disturbance and will be neglected. In addition, considering that the losses in the converter are small, in steady state, it can be written as:

$$i_r v_{dc} \cong i_r v_{dc}^* = \frac{3}{2} V_d i_d \quad (3.16)$$

It is considered that the dynamics of the current control loop is fast enough. Thus, in the analysis of the external loop, its dynamics can be neglected. Using a PI controller, the following closed-loop transfer function is obtained:

$$\frac{v_{dc}(s)}{v_{dc}^*(s)} = \frac{K k_{p,dc} s + K k_{i,dc}}{C_{dc} s^2 + K k_{p,dc} s + K k_{i,dc}} \quad (3.17)$$

where $K = \frac{3}{2} \frac{V_d}{v_{dc}^*}$, $k_{p,dc}$ and $k_{i,dc}$ are the proportional and integral gains of the d.c. bus voltage, respectively. The controller setting is performed by the pole allocation method. The controller gains are set so that both poles of the closed loop transfer function of the system are real. This way:

$$k_{p,dc} = \frac{2\pi(f_{dc1} + f_{dc2})C_{dc}}{K} \quad (3.18)$$

$$k_{i,dc} = \frac{4\pi^2 f_{dc1} f_{dc2} C_{dc}}{K} \quad (3.19)$$

where f_{dc1} and f_{dc2} are the frequencies of the poles (closed loop). Typically, these poles are spaced apart from each other by a decade and the value of the largest of them must be allocated at least a decade below the cutoff frequency of the current loop. This ensures proper operation of the cascade control.

The control of the injected reactive power is performed considering that, in the presence of PLL, $V_q = 0$. If we neglect the dynamics of the internal current loop and consider a PI controller, we can obtain:

$$\frac{Q(s)}{Q^*(s)} = \frac{H(k_{p,Q} s + k_{i,Q})}{(1 + H k_{p,Q}) s + H k_{i,Q}} \quad (3.20)$$

where $H = -\frac{3}{2} V_d$, $k_{p,dc}$ and $k_{i,dc}$ are the proportional and integral gains of

the reactive power loop, respectively. By using pole allocation, the gains are calculated as:

$$k_{p,Q} = \frac{2\pi f_{q2}}{2\pi H(f_{q1} - f_{q2})} \quad (3.21)$$

$$k_{i,Q} = 2\pi f_{q1} k_{q,Q} \quad (3.22)$$

where f_{q1} and f_{q2} are the frequencies of the poles of the closed loop. Again, these poles are spaced apart from each other for a decade and the value of the largest of them must be allocated at least a decade below the cut-off frequency of the current loop.

Adjustment of the Parameters Used in the Tests

To validate the three SAS models, simulations were performed in Matlab/Simulink and PLECS. In this chapter, the parameters are chosen to validate the proposed structures by using market values. Thus, the following steps are taken:

- An arrangement and a panel model from the solar panel industry is chosen;
- A three-phase photovoltaic inverter is presented to be used in the validation test;
- Two case studies are presented in order to validate the proposed structure.

The first step is to choose a panel model. Thus, an arrangement with 2 strings of 20 panels Komaes KM 250 Wp was simulated. Such an arrangement results in an open circuit voltage of 750 V and a current of 17 A. The curve data of this arrangement are inserted in a look-up table that is used in the current control of the emulator.

The SAS parameters are set to obtain the values of the chosen solar panel. Using the methods and equations given in the previous chapter, the parameters are calculated.

The Table 4.1 shows some values of voltage source and resistance for different values of temperature and irradiance used in SAS based on Thevenin's Circuit, where:

$$V_{eq} = 2V_{MPPT} \quad (4.1)$$

$$R_{eq} = \frac{V_{MPPT}}{I_{MPPT}} \quad (4.2)$$

where v_s and i_L are the output voltage and current of the panel model, respectively.

Tabela 4.1: Parameters of the solar panel

Temp ($^{\circ}C$)	Irrad (W/m^2)	V_s (V)	I_L (A)	R_{eq} (Ω)	V_{eq} (V)	P (W)
25	100	915	0.74	1242	1830	674
	200	950	1.54	616	1900	1464
	300	967	2.35	412	1935	2271
	400	978	3.15	310	1957	3085
	500	986	3.96	249	1972	3904
	600	991	4.77	208	1982	4724
	700	995	5.57	179	1990	5544
	800	998	6.38	156	1995	6362
	900	999	7.18	139	1999	7180
	1000	1001	8.00	125	2001	8004
35	1000	903	7.97	113	1805	7194
45	1000	806	7.94	101	1611	6397
55	1000	710	7.89	90	1420	5601

The Table 4.2 shows the parameters for SAS based on buck converter.

The Table 4.3 shows the parameters for SAS based on PWM + buck converter.

4.1 PV Inverter Model

A three-phase photovoltaic inverter is used in this work. It is a 10 kW with an LCL filter connected to the power grid, as shown in Fig. 4.1. The system uses an IGBT bridge to transform the d.c. current of the PV panels

Tabela 4.2: D.c./d.c. Stage Parameters

Parameters	Symbol	Value
Switching frequency	f_{sb}	30 kHz
Inductance	L_b	0.115 mH
Inductor resistance	R_{Lb}	1.09 Ω
Capacitance	C_s	0.3 mH
Prop. gain of current loop	$k_{p,iL}$	2.89 A/K
Int. gain of current loop	$k_{i,iL}$	27.24 A/K
Prop. gain of voltage loop	$k_{p,vs}$	0.62 V/K
Int. gain of voltage loop	$k_{i,vs}$	10.6 V/K

in alternated current. An LCL filter connects the converter to the grid in order to mitigate the switching frequency harmonics.

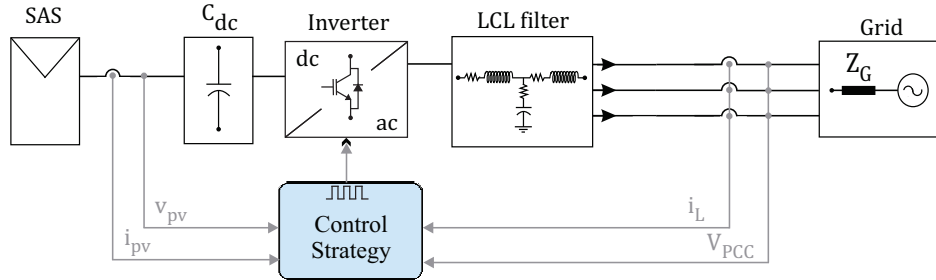


Figura 4.1: Grid-connected photovoltaic system based on three-phase multifunctional inverter

The complete control structure is shown in Fig. 4.2 The control strategy is based on the grid side current measurement and the dc-link voltage control is based on the voltage-squared control method.

Tabela 4.3: A.c./a.c. Stage Parameters

Parameters	Symbol	Value
Maximum power	P_{max}	10 kW
Grid Voltage	V_g	220 V
Grid Frequency	f_n	60 Hz
Dc-link Voltage	V_{dc}	750 V
Switching Frequency	f_s	30 kHz
Filter Inductance	L_f	0.81 mH
Filter Resistance	R_f	60 Ω
Dc-link Capacitance	C_{dcc}	3.06 mF
Prop. gain of grid current loop	$k_{p,idq}$	6 A/K
Int. gain of grid current loop	$k_{i,idq}$	75 A/K
Prop. gain of dc-link voltage loop	$k_{p,vdc}$	1.4 V/K
Int. gain of dc-link voltage loop	$k_{i,vdc}$	32 V/K

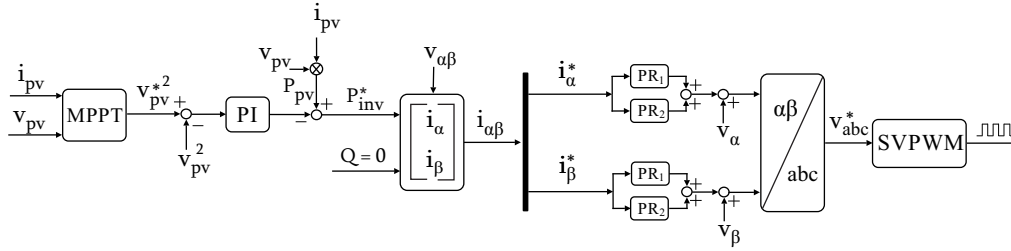


Figura 4.2: Complete inverter control strategy

Neglecting the effect of the capacitor in filter on the fundamental frequency and considering a three phase balanced system, dynamic of the inverter in $\alpha\beta$ coordinate is given by:

$$v_\alpha - R_{i\alpha} - L \frac{di_\alpha}{dt} - V_\alpha = 0, \quad (4.3)$$

$$v_\beta - R_{i\beta} - L \frac{di_\beta}{dt} - V_\beta = 0, \quad (4.4)$$

where L represents the sum of the filter inductance and R is the sum of the filter resistances.

The squared reference dc-bus voltage used in the outer control loop, is generated by a maximum power point tracker algorithm (MPPT), based on incremental conductance. The behavior of the dc-bus capacitor can be represented by the energy storage (W) stored in its terminals, i.e.

$$W = \frac{1}{2}C_{dc}v_{pv}^2 \quad (4.5)$$

The time derivative of the W represents the instantaneous power stored in the capacitor p_{cap} . Thus, the injected power by the inverter (p_{inv}) is given by:

$$p_{inv} = p_{pv} + p_{cap}, \quad (4.6)$$

Thus, the relation between p_{cap} and v_{pv} is expressed by:

$$v_{pv}^2 = \frac{p_{cap}}{2C_{dc}s}, \quad (4.7)$$

Thereby, considering the ideal inner loop, the outer closed-loop (G_{out}) is obtained

$$G_{out} = \frac{v_{pv}^2}{v_{pv}^{*2}} = \frac{2k_p(\tau_i s + 2)}{\tau_i C_{dc} s^2 + 2k_p(\tau_i s + 2)}, \quad (4.8)$$

where k_p and τ_i are the PI controller parameters. The poles allocation method is used to tune the PI controller, ensuring a desired response of the dc-bus voltage.

The average reactive power q of the load is detected through the instantaneous power theory (IPT) and saturated, generating q^* . Thus, with the powers p_{inv} , q and PCC voltage $v_{\alpha\beta}$, the fundamental components i_α and i_β of the load current is obtained

$$\begin{bmatrix} i_\alpha \\ i_\beta \end{bmatrix} = \frac{1}{v_\alpha^2 + v_\beta^2} \begin{bmatrix} p_{inv} \\ q^* \end{bmatrix} \quad (4.9)$$

The proportional multi-resonant (PMR) controller of the current is tuned

in each frequency of the inverter current reference. This controller calculates the converter modulation index v_{abc} to set the converter switches pulses through the SVPWM algorithm.

4.2 Studies Applied to Test the SAS

Two test conditions are presented in order to validate the proposed structure. In the first condition, the SAS is subjected to a profile irradiance variation, where initially the irradiance starts at 1000 W/m^2 , falling to 600 W/m^2 and finally to 200 W/m^2 , keeping its temperature at $25 \text{ }^\circ\text{C}$.

In the second condition, the SAS emulates a variation in the PV temperature. Initially the temperature starts at $20 \text{ }^\circ\text{C}$, increasing to $30 \text{ }^\circ\text{C}$, and after to 40°C keeping the irradiance at 1000 W/m^2 .

In both cases, the three SAS models should be able to follow the mathematical model (shown in chapter 2) reference. With the accomplishment of these tests, besides verifying the values of current and voltage in the SAS output, it is possible to evaluate the sensitivity to the variation of irradiance and temperature.

Results

In this chapter, the results from the case study are shown and analyzed. The results for the three SAS are compared with the mathematical model results in both cases: irradiance and temperature variation. Besides showing the current, voltage and power at the SAS output, the maximum power point curve is also plotted during the irradiance variation. At last, a discussion about the results is made and, then, a general analysis is performed.

5.1 Simulation Results

5.1.1 Irradiance Variation

In Fig. 5.1 (a), it can be seen the voltage performance of the three SAS models subjected to irradiance variation ($1000/600/200 \text{ W/m}^2$). It is observed that the behavior does not change; however, in Fig. 5.1 (b), it is observed that the topology of Buck converter presents more oscillations, i.e. in this case the MPPT dynamics of the inverter under test is more affected, providing a topology with ripples in the output current greater than the others. It happens because the MPPT is always trying to adjust the current value, for example, to the defined value. As power is given by current multiplied by voltage, the ripples of the current is reflected in Fig. 5.1 (c). Thus, it is observe a very similar performance for the three topologies in question of delivered power.

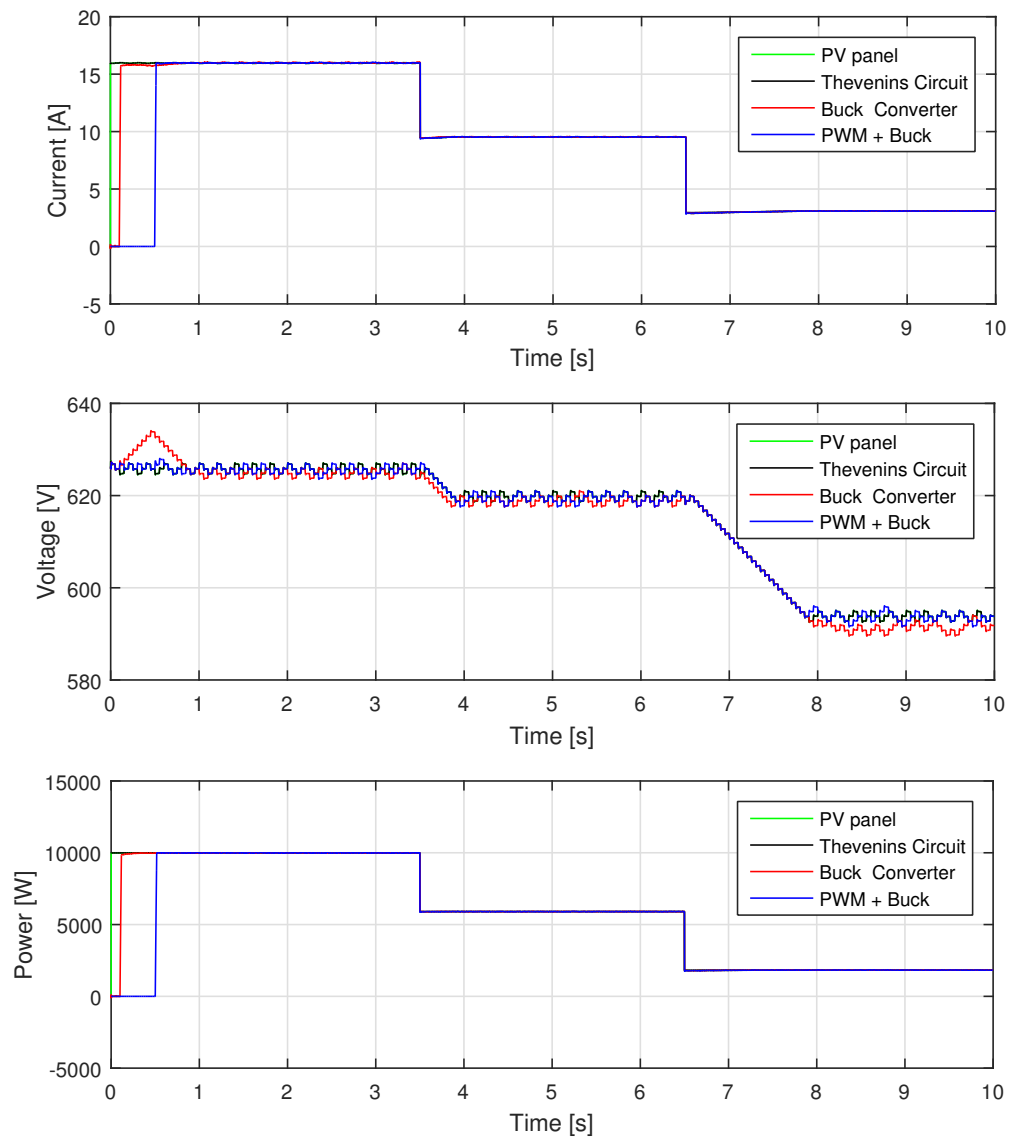


Figure 5.1: Electrical Variables of the Artificial Panel during a variation of irradiance and constant temperature (25°C). (a) SAS output current. (b) SAS output voltage. (c) SAS output power.

Fig. 5.2 shows the performance of the SAS models when subjected to temperature variation (20°C to 30°C to 40°C). Fig. 5.2 (a), (b) and (c) represent the voltage, current and power, respectively. Due to the linearized model of the panel based on the Thévenin circuit, the output voltage reflects this linear model. Its output does not accurately follow the model of a photovoltaic panel, and thus shows a lower sensitivity to temperature change than the panel based on the buck converter. However, the time for stabilization is the same for all three models.

Fig. 5.3 shows the dynamics for the three types of artificial panels in the $P \times V$ plane. In terms of performance the three are very similar, the models differ somewhat in the transition from the first stage, when the irradiance is equal to 1000 W/m^2 for the second, when the irradiance is 600 W/m^2 . However, they all show a good approximation to the maximum power point.

That result is very important once the main PV inverter function is injecting the maximum generated power into the power system.

This last analysis shows the transient response of the three proposed models since they are able to reach the maximum power point.

5.2 Discussion

As can be seen in the simulation results, all SAS topologies were able to follow the mathematical model. In the first case, irradiance variation, the three models reached the expected current, voltage and power values. In addition, the three models presented sensitivity and speed in the alteration of this irradiance. Thus, the three SAS models were successful in the first condition.

For the temperature variation, all the models also managed to achieve the expected result. Although the Thevenin model stabilized faster after the temperature change, the result of the other two models did not compromise its performance. Then, all three models passed this second test.

In the last test, it was shown the capacity of reaching the maximum power point. The SAS models were able to reach this point. All of the SAS can emulate the array I-V curve and the tested. There is a delay between the

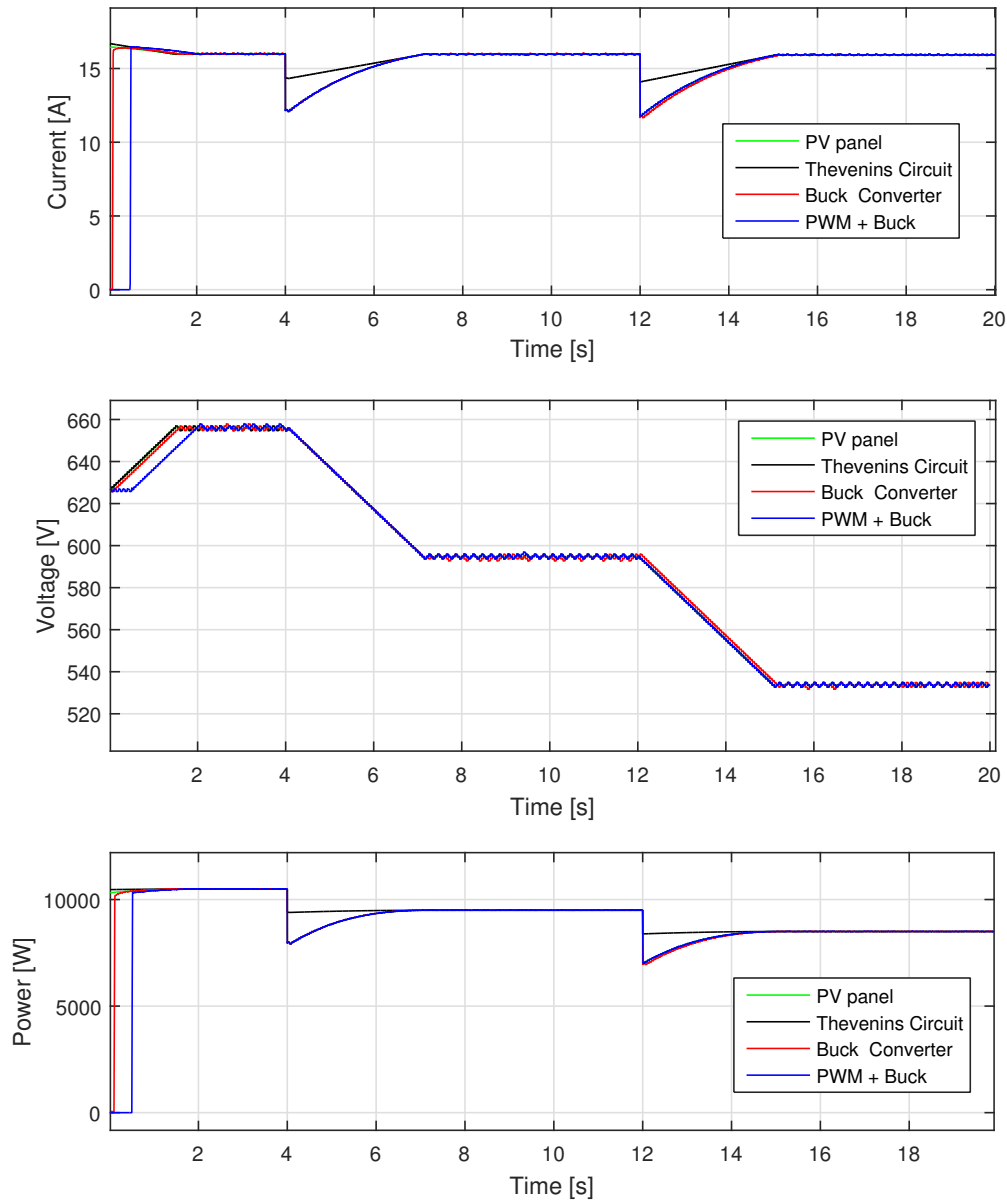


Figura 5.2: Electrical variables of the artificial panels during a temperature variation (20°C to 30°C to 40°C) and constant irradiance ($1000\text{ W}/\text{m}^2$). (a) SAS Output current. (b) SAS Output voltage. (c) SAS Output power.

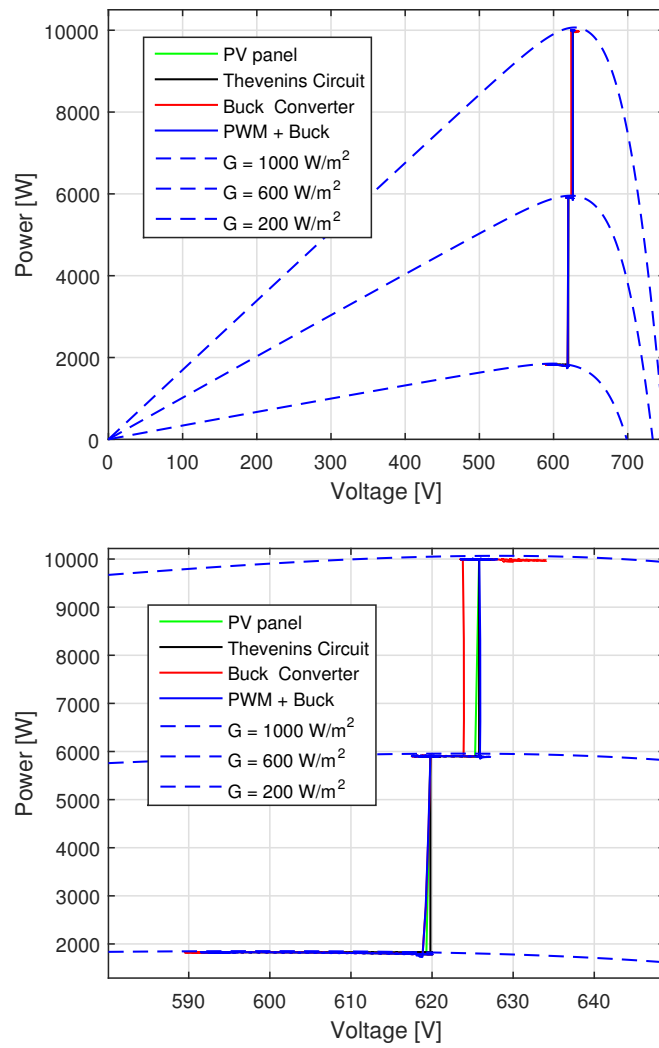


Figura 5.3: (a) SAS track during the test of a photovoltaic converter in the P x V plane. (b) maximum power point zoom.

models in the beginning of the simulations due to some technical adjustments. Some switches were used to avoid peak current at initialization.

5.3 General Analysis

Through the results, SAS has been able to effectively emulate the behavior of a real solar panel. The difference between their outputs values are very small. Then, the best way to differentiate them when choosing which one to use is through their topologies.

SAS based on Thevenin's Circuit is the simplest presented model. This model has a lower manufacturing cost. Thus, it is the best option when resources are scarce. However, the losses in this model are higher than in the others, and it has items with limitations (e.g., d.c. source). This SAS based on Thevenin's Circuit should be used in low power applications.

SAS Based on buck converter has the d.c. source limitation. Since this is an expensive device, the fabrication of this model becomes more complex. It has fewer losses, and it is a safer option. This SAS should be used in low power applications due its d.c. source.

SAS Based on PWM Rectifier and Buck Converter can be used in high power applications. Although it has switching losses, it also has a high current capacity.

Conclusion

In this work, four models of photovoltaic arrangements were presented. The first one is the mathematical model defined as reference model, and the other three are artificial panels (Solar Array Simulator). The work sought to contribute by showing three alternative topologies that imitate a real photovoltaic panel for PV inverter tests for certification. The work tries to find models with greater efficiency and best sensitivity to meteorological changes. The modeling and design of the controllers were presented, as well as the results of the simulations.

It was observed that the topology based on the buck converter has more ripples than the one based on the Thevenin circuit. On the other hand, the panel based on the Thevenin's circuit has high losses. Both models presented operational advantages being able to emulate the characteristics of the photovoltaic arrangement. The trajectories obtained in the $P \times V$ plane also showed the inverter's ability to track the emulator's maximum power point.

Another positive point for the Thevenin circuit is the simple topology compared to the model based on the buck converter. However, this model may have a great loss in practice due to the presence of the resistor at the output of the artificial panel. Future work on this topic may include an analysis of cost, loss and useful life. Then, with the results of this work, it can be concluded that all presented topologies perform with satisfying the role of artificial panel.

In this way, this work shows the versatility of the photovoltaic system proposing an improvement in the method of inverter test. Currently, the biggest obstacle to the growth of photovoltaic technology is the lack of equipment with genuinely Brazilian technology, once imported equipment has a high cost. The proposed SAS is a tool that can contribute to this technological growth in the country.

Future Work

Future works can provide a detailed analysis of each technique emphasizing on its:

- Realization cost
- Accuracy
- Level of complexity
- Hardware implementation
- Efficiency.

This way, a comparison between the models can be done to decide each one is the best to be used in residential PV inverter test, for example.

6.1 Published Works

- E. G. de Andrade, H. A. de Oliveira, W. V. Ribeiro, R. C. de Barros, H. A. Pereira and A. F. Cupertino, "Power losses in photovoltaic inverter components due to reactive power injection,"2016 12th IEEE International Conference on Industry Applications (INDUSCON), Curitiba, 2016, pp. 1-7.
- G. L. E. Mata, R. C. de Barros, W. V. Ribeiro, L. S. Xavier, A. F. Cupertino and H. A. Pereira, "LCL filter losses due to harmonic compensation in a photovoltaic system,"2017 IEEE 8th International Symposium on Power Electronics for Distributed Generation Systems (PEDG), Florianopolis, 2017, pp. 1-7.

- R. C. de Barros, W. V. Ribeiro, G. L. E. Mata, L. S. Xavier, A. F. Cupertino and H. A. Pereira, "Design of a current harmonic detector method applied in photovoltaic inverters with ancillary service capability," 2017 IEEE 8th International Symposium on Power Electronics for Distributed Generation Systems (PEDG), Florianopolis, 2017, pp. 1-7.
- R. M. Paulo, L. A. R. Rios, W. V. Ribeiro, A. F. Cupertino and H. A. Pereira, "Performance comparison of IGBTs and SiC-MOSFET applied in photovoltaic inverters during reactive power injection," 2017 Brazilian Power Electronics Conference (COBEP), Juiz de Fora, 2017, pp. 1-6.
- W. V. Ribeiro, H. A. Pereira, A. F. Cupertino, Shirley P. Freitas and Victor F. Mendes, "Comparação Entre Topologias De Painel Solar Artificial Para Teste De Inversores Fotovoltaicos", VII Congresso Brasileiro de Energia Solar - CBENS, Gramado, 2018, pp. 1-9.
- R. C. de Barros, W. V. Ribeiro, H. A. Pereira, A. F. Cupertino, "Métodos de discretização aplicados no detector de corrente harmônica baseado na estrutura da SOGI-PLL: um estudo comparativo", VII Congresso Brasileiro de Energia Solar - CBENS, Gramado, 2018, pp. 1-9.

Referências Bibliográficas

- Babu, T. S., Ram, J. P., Sangeetha, K., Laudani, A., and Rajasekar, N. (2016). Parameter extraction of two diode solar pv model using fireworks algorithm. *Solar Energy*, 140:265–276.
- Bower, W., Whitaker, C., Erdman, W., Behnke, M., and Fitzgerald, M. (2004). Performance test protocol for evaluating inverters used in grid-connected photovoltaic systems. *Sandia National Laboratories*.
- Boyson, W. E., Galbraith, G. M., King, D. L., and Gonzalez, S. (2007). Performance model for grid-connected photovoltaic inverters. Technical report, Sandia National Laboratories.
- Bun, L., Raison, B., Rostaing, G., Bacha, S., Rumeau, A., and Labonne, A. (2011). Development of a real time photovoltaic simulator in normal and abnormal operations. In *IECON 2011-37th Annual Conference on IEEE Industrial Electronics Society*, pages 867–872. IEEE.
- Camino-Villacorta, M., Egido-Aguilera, M. A., and Díaz, P. (2012). Test procedures for maximum power point tracking charge controllers characterization. *Progress in Photovoltaics: Research and Applications*, 20(3):310–320.
- Cupertino, A., De Resende, J., Pereira, H., and Júnior, S. S. (2012). A grid-connected photovoltaic system with a maximum power point tracker using passivity-based control applied in a boost converter. In *Industry Applications (INDUSCON), 2012 10th IEEE/IAS International Conference on*, pages 1–8. IEEE.

- Cupertino, A. F., Pereira, H. A., and Mendes, V. F. (2017). Modeling, design and control of a solar array simulator based on two-stage converters. *Journal of Control, Automation and Electrical Systems*, 28(5):585–596.
- Cupertino, A. F., Santos, G. V., Pereira, H. A., Silva, S. R., and Mendes, V. F. (2015). Modeling and control of a flexible photovoltaic array simulator. In *Industrial Electronics (ISIE), 2015 IEEE 24th International Symposium on*, pages 318–324. IEEE.
- De Soto, W., Klein, S., and Beckman, W. (2006). Improvement and validation of a model for photovoltaic array performance. *Solar energy*, 80(1):78–88.
- Di Piazza, M. C., Pucci, M., Ragusa, A., and Vitale, G. (2010). Analytical versus neural real-time simulation of a photovoltaic generator based on a dc–dc converter. *IEEE Transactions on Industry Applications*, 46(6):2501–2510.
- EPIA, Masson, G., Latour, M., Rekinge, M., Theologitis, I.-T., and Papoutsis, M. (2017). Global market outlook for photovoltaics 2017, epia.
- Erickson, R. W. and Maksimovic, D. (2007). *Fundamentals of power electronics*. Springer Science & Business Media.
- Gadelovits, S., Sitbon, M., and Kuperman, A. (2014). Rapid prototyping of a low-cost solar array simulator using an off-the-shelf dc power supply. *IEEE Transactions on Power Electronics*, 29(10):5278–5284.
- Gonzalez, S., Kuszmaul, S., Deuel, D., and Lucca, R. (2010). Pv array simulator development and validation. In *2010 35th IEEE Photovoltaic Specialists Conference*, pages 002849–002852.
- Liserre, M., Blaabjerg, F., and Hansen, S. (2001). Design and control of an lcl-filter based three-phase active rectifier. In *Industry Applications Conference, 2001. Thirty-Sixth IAS Annual Meeting. Conference Record of the 2001 IEEE*, volume 1, pages 299–307. IEEE.
- Matsukawa, H., Koshiishi, K., Koizumi, H., Kurokawa, K., Hamada, M., and Bo, L. (2003). Dynamic evaluation of maximum power point tracking operation with pv array simulator. *Solar Energy Materials and Solar Cells*, 75(3-4):537–546.

- Nagayoshi, H. (2004). I–v curve simulation by multi-module simulator using i–v magnifier circuit. *Solar energy materials and solar cells*, 82(1-2):159–167.
- Ollila, J. (1995). A medium power pv-array simulator with a robust control strategy. In *Control Applications, 1995., Proceedings of the 4th IEEE Conference on*, pages 40–45. IEEE.
- Pandey, A., Dasgupta, N., and Mukerjee, A. K. (2007). A simple single-sensor mppt solution. *IEEE Transactions on Power Electronics*, 22(2):698–700.
- Piao, Z. G., Gong, S. J., An, Y. H., and Cho, G. B. (2013). A study on the pv simulator using equivalent circuit model and look-up table hybrid method. In *Electrical Machines and Systems (ICEMS), 2013 International Conference on*, pages 2128–2131. IEEE.
- Ponnaluri, S., Krishnamurthy, V., and Kanetkar, V. (2000). Generalized system design and analysis of pwm based power electronic converters. In *Industry applications conference, 2000. Conference record of the 2000 IEEE*, volume 3, pages 1972–1979. IEEE.
- Rauschenbach, H. S. (2012). *Solar cell array design handbook: the principles and technology of photovoltaic energy conversion*. Springer Science & Business Media.
- Rodriguez, P., Teodorescu, R., Candela, I., Timbus, A. V., Liserre, M., and Blaabjerg, F. (2006). New positive-sequence voltage detector for grid synchronization of power converters under faulty grid conditions. In *Power Electronics Specialists Conference, 2006. PESC'06. 37th IEEE*, pages 1–7. IEEE.
- Solanki, C. S. (2015). *Solar photovoltaics: fundamentals, technologies and applications*. PHI Learning Pvt. Ltd.
- Soltau, N., Shen, Z., and De Doncker, R. W. (2015). Design of series inductances for high-power dc-dc converters. In *Renewable Energy Research and Applications (ICRERA), 2015 International Conference on*, pages 890–895. IEEE.

- Souza, L., Cortizo, C., and Mendes, A. (2013). Study and design of a photovoltaic array simulator. In *Power Electronics Conference (COBEP), 2013 Brazilian*, pages 544–549. IEEE.
- Vijayakumari, A., Devarajan, A., and Devarajan, N. (2012). Design and development of a model-based hardware simulator for photovoltaic array. *International Journal of Electrical Power & Energy Systems*, 43(1):40–46.
- Villalva, M. G., Gazoli, J. R., and Ruppert Filho, E. (2009). Comprehensive approach to modeling and simulation of photovoltaic arrays. *IEEE Transactions on power electronics*, 24(5):1198–1208.